THIN CURRENT SHEETS IN THE DEEP GEOMAGNETIC TAIL

T. I. Pulkkinen

Finnish Meteorological Institute, Helsinki, Finland

D. N. Baker and C. J. Owen

NASA/Goddard Space Flight Center, Greenbelt, MD

J. T. Gosling

Los Alamos National Laboratory, Los Alamos, NM

N. Murphy

Jet Propulsion Laboratory, Pasadena, CA

Abstract. The ISEE-3 magnetic field and plasma electron data from Jan - March 1983 have been searched to study thin current sheets in the deep tail region. 33 events were selected where the spacecraft crossed through the current sheet from lobe to lobe within 15 minutes. The average thickness of the observed current sheets was $2.45R_E$, and in 24 cases the current sheet was thinner than $3.0R_E$; 6 very thin current sheets (thickness $\lambda < 0.5R_E$) were found. The electron data show that the very thin current sheets are associated with considerable temperature anisotropy. On average, the electron gradient current was $\sim 17\%$ of the total current, whereas the current arising from the electron temperature anisotropy varied between $8-45\%$ of the total current determined from the lobe field magnitude.

Introduction

Very thin current sheets with thickness of the order of the ion Larmor radius or less have frequently been observed in the near-Earth tail in association with substorm activity [McPherron et al., 1987]. During the growth phase close to the inner edge of the plasma sheet [Baker and McPherron, 1990] and in the expansive phase throughout the mid-tail region [Fairfield et al., 1981] these thin sheets are thought to play a key role in the dynamical sequence of substorms. However, the strong gradients along the tail axis and the rapid temporal changes of the magnetospheric configuration during the substorm evolution make a detailed study of the properties of such thin current sheets difficult.

At large geocentric distances the magnetic field configuration becomes much more one-dimensional [Slavin et al., 1985] and, outside of periods of strong magnetic activity, may remain time-stationary for relatively long periods. During early 1983 the International Sun-Earth Explorer 3 (ISEE 3) satellite was in the distant tail ($X < -200R_E$ in geocentric solar magnetospheric (GSM) coordinates, in which X is along the Sun-Earth line, Z in the plane defined by X and the dipole axis, and Y completes the right handed triad) and probed the electron plasma and magnetic field configuration of the central parts of the geomagnetic tail. In this paper we show that in many cases the current sheet in the distant tail is well defined and very thin, and that the observed configurations often resemble those inferred to occur in the near-Earth region during periods of magnetic activity. We present statistical results of the magnetic field and plasma electron properties of 33 current sheet crossings where magnetic field and electron data were available and for which the current sheet thickness could be determined. In the final section, we compare and contrast these results with the substorm-associated thin current sheets.

Event Selection

In order to examine thin current sheets in the deep tail, we looked for events where ISEE 3 passed from one lobe to the other within a few (< 15) minutes. Magnetic field [Frandsen et al., 1978] and electron plasma [Bame et al., 1978] summary plots from January 1983 were scanned to identify periods when rapid traversals of the tail current sheet occurred with lobe signatures on each side of the crossing. Cases where the satellite entered the magnetosheath on either side of the current sheet were not included. The different regions of the tail (north lobe, south lobe, current sheet) were identified by sunward (anti-sunward) field and low temperature in the north (south) lobe, and small field magnitude and higher temperature in the current sheet [Zwickl et al., 1984]. Some previously studied events from February and March of 1983 were added to the list [Gosling et al., 1985], which then totaled 48 events.

Data from the energetic particle anisotropy spectrometer (EPAS) on ISEE 3 [Balogh et al., 1978] was used to estimate the velocity of the current sheet for each case, using the method employed by Murphy et al. [1987]. This method determines the speed at which the edge of the plasma sheet boundary layer crosses the spacecraft position either prior to and/or after the current sheet encounter. Assuming uniform motion of the tail structures, the thickness of the current sheet is then inferred from the duration of the encounter. We were able to make an estimate of the boundary velocities for 33 of the 48 current sheet events. For the other events, the spacecraft was either located within the plasma sheet boundary layer for some time prior to and/or after the crossing (and hence there was no encounter with the edge of that layer), or analysis did not yield results consistent with a planar boundary rapidly crossing the spacecraft position.

Figure 1 shows data from 2115 to 2145 UT on 21 January 1983 which contains a current sheet crossing typical of those in the data set. The spacecraft was located in the south lobe of the tail at $(-205.1, -6.2, -6.9)R_E$. The top four panels show the magnetic field
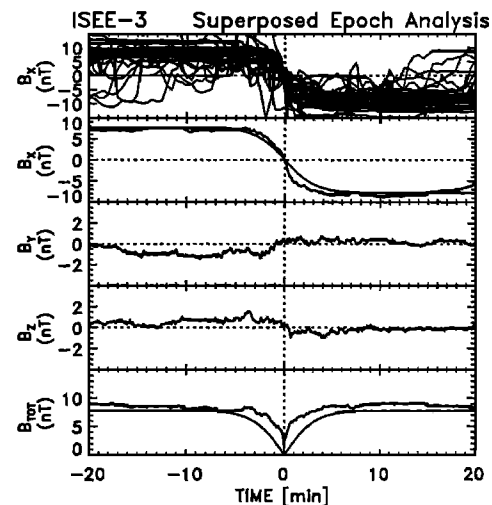

Fig. 1. ISEE 3 current sheet crossing on 21 January 1983 at 2131 UT. Panels from top to bottom: Magnetic field components B_X, B_Y, B_Z, and $|B|$ in GSM-coordinates, flow velocity, and temperature anisotropy T_{MAX}/T_{MIN}.

components in GSM-coordinates. A Harris field model for the magnetic field X-component $B_X = B_0 \tanh[U \cdot (t - t_0)/\lambda]$, where the lobe magnetic field intensity is $B_0 = 6.7$nT, the boundary velocity $U = 45.5$km/s, and current sheet thickness $\lambda = 0.34R_E$, has been superposed on the measured B_X and field magnitude plots. The bulk electron velocity was quite typical, below 600km/s, and the electron temperature anisotropy (ratio of the temperatures in the direction of the maximum and minimum temperatures) was slightly above 1.2, somewhat above the average in this set of events. The direction of the temperature maximum (data not shown) reveals that the temperature parallel to the magnetic field was greater than the temperature in the perpendicular direction. The current sheet passed over the spacecraft at a speed of 45.5km/s in about 2 minutes. The event occurred during relatively quiet geomagnetic conditions as determined from the AE-index, about 30 minutes after the complete recovery of a 500 nT substorm (onset at ~1840 UT).

The events were selected without reference to magnetic activity. Dependences of the current sheet characteristics on magnetic activity were studied using 1-hour averaged AE-index. The very thin current sheet observations were, except for one, all made during very low magnetic activity (AE < 100nT). Otherwise, there was practically no correlation between AE and current sheet thickness. Only a slight tendency for larger current sheet thicknesses during magnetically active periods was observed.

Current Sheet Thickness Estimates

The current sheet thicknesses for the 33 events were estimated two different ways. Both methods utilized the boundary velocity U obtained from the energetic ion data. In cases where both entry and exit speeds were obtained, the average value was used in the current sheet thickness estimation.

High-resolution (3-second averaged) magnetic field data was used to determine the time period Δt of depressed field magnitude during the current sheet crossings. The current sheet thickness was then estimated from $\lambda = U \cdot \Delta t$. The average thickness using this estimate was 2.7R_E. In 22 events out of 33 the current sheet thickness was less than 3.0R_E.

The Harris model magnetic field was used to describe the X-component of the observed magnetic field. The optimal fit to the data was determined by a least squares fitting procedure, minimizing the error with respect to both lobe field strength B_0 and current sheet thickness λ. In this case, the average thickness was 2.2R_E, and there were 26 events with current sheet thickness less than 3.0R_E.

The error involved with the velocity estimates was relatively large, of the order of ±10km/s. We assume that the error in the time estimate Δt in the first thickness estimate is less than 30 seconds, which gives an error in the final current sheet thickness ~ 0.4R_E for the thin current sheet crossings ($\lambda < 3.0R_E$), and ~ 0.8R_E for all 33 events. If we assume that the least squares sum of the X-components of the field is proportional to the error in B_X, the resulting error in the second thickness estimate gives very similar results, 0.3R_E and 0.8R_E for thin crossings and all crossings, respectively.

In the following analysis we have used an average of the current sheet thicknesses given by these two methods. The average gave a value of 2.45R_E, and 24 events had a mean current sheet thickness less than 3.0R_E. We define these as thin crossings (Figure 2). For the 24 events, the two results deviated from the average value by ~ 0.3R_E, whereas the deviation for all 33 events is much larger, ~ 0.8R_E. Thus within the accuracy of the thickness determination, the two methods gave similar results. The thick current sheets were often characterized by multiple crossings and complex behavior, which increased the differences in the thickness estimates. Six very thin current sheets with thickness less than 0.5R_E were found. In all these cases the current sheet velocity relative to the spacecraft was rather slow, in addition to very short crossing time lasting only a few minutes.

Plasma Electron Properties

The plasma electron data were available for all the selected current sheet crossings. ISEE 3 made 3 s snapshots of the electron velocity distribution functions (8.5 − 1140 eV), usually at intervals of ~ 84 s, which for rapid crossings gives only a few measurements in the current sheet region, thus limiting the possibilities of a more detailed study.
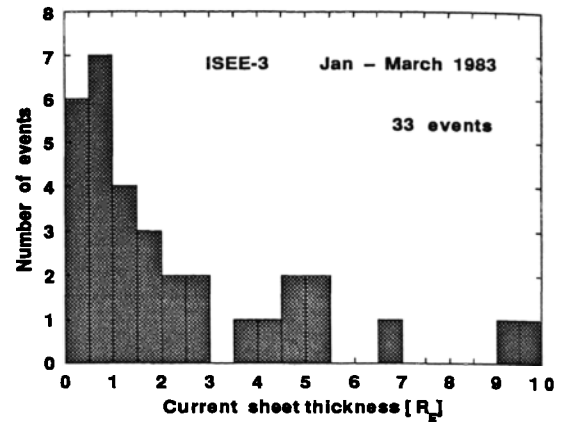

Fig. 2. Histogram of current sheet thickness distribution for all 33 events. The crossings are binned in 0.5 R_E bins.

Both two- and three-dimensional measurements were made. Two-dimensional sweeps in the ecliptic plane sample most pitch-angles in the deep-tail one-dimensional current sheet geometry. Thus, the electron temperature anisotropies were well determined. The electron bulk flow measurements were subject to some uncertainties due to imperfect photoelectron and spacecraft charging compensation [e.g. Bame et al., 1978; Zwickl et al., 1984]. There can also sometimes be field-aligned current contributions to the inferred flow velocity, but evidence suggests that the plasma direction and speed determination by ISEE 3 was reasonably well determined above ~ 100km/s [Zwickl et al., 1984].

The electron plasma flow velocity was tailward in all but 3 of the 33 events, suggesting that the spacecraft was tailward of the distant neutral line during the selected periods [Slavin et al., 1985]. Figure 3a shows the current sheet thickness distributions when the events have been categorized according to flow velocity. Large flow velocity ($| V_X | > 300$km/s) was observed in 19 events. The thin current sheets ($\lambda < 3.0R_E$) were typically associated with smaller flow velocities than were observed in the events where the current sheet was thicker. This further supports the conclusion that the thin current sheets are stable structures associated with relatively quiet magnetic conditions, whereas the thick sheets with fast tailward flows have been suggested to be associated with plasmoid events during magnetospheric substorms [Baker et al., 1987]. The very thin current sheet
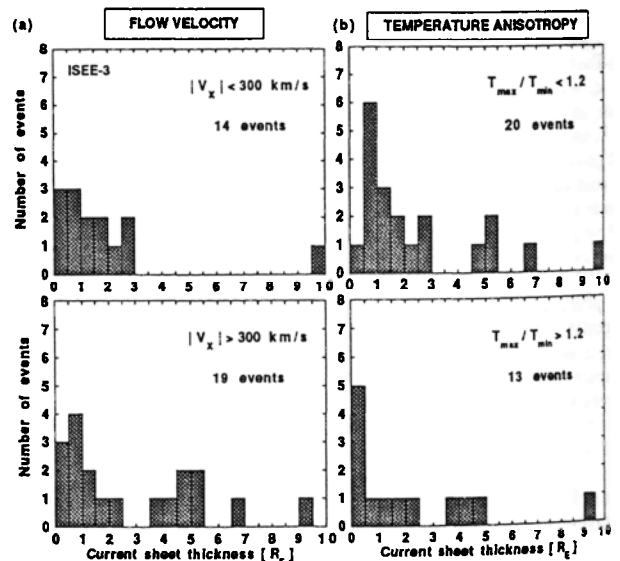

Fig. 3. Histogram of current sheet thickness distribution for a) slow flow velocity ($V_X < 300$km/s) events and large flow velocity ($V_X >$ 300km/s) events, b) selected 'isotropic' ($T_{MAX}/T_{MIN} < 1.2$) events and selected 'anisotropic' ($T_{MAX}/T_{MIN} > 1.2$) events. The crossings are binned in 0.5R_E bins.

events (λ < 0.5R$_E$) were associated with moderate flow velocities varying from 0 to 400km/s.

The average electron temperatures in the maximum and minimum directions were calculated over the period the satellite was within the current sheet. In 13 events the temperature anisotropy (T_{MAX}/T_{MIN}) was larger than 1.2 during the current sheet crossings. As most of the events showed some degree of anisotropy, T_{MAX}/T_{MIN} = 1.2 has been used to divide events into 'isotropic' and 'anisotropic' classes. As noted above, the direction of the anisotropy was such that the temperature parallel to the magnetic field was larger than the perpendicular component. Generally, the isotropic events were more frequent in the thin current sheet crossings, whereas the anisotropic events showed no clear correlation with the current sheet thickness (Figure 3b). However, 5 out of the 6 very thin current sheets were associated with relatively large temperature anisotropy.

Superposed Epoch Analysis

In order to study the average characteristics of the magnetic field behavior, data from all 33 crossings have been combined to form a superposed epoch time series (Figure 4). The events have been combined by coinciding the minimum | B | closest to the sign reversal of B_X. For the X and Y components, $-B_X$ and $-B_Y$ have been used for south-to-north crossings, whereas the Z components have not been reversed. The top panel of Figure 4 shows the individual X-components of all events, with $-B_X$ plotted for the south-to-north crossings. The next four panels show the GSM-components of the superposed epoch field as well as the field magnitude. A Harris field model with average velocity 82.7km/s, average thickness λ = 2.45R$_E$, and average lobe field strength 7.8nT has been superposed on the X-component and field magnitude plots.

Both B_Y and B_Z show a wavy structure with a sign reversal at the current sheet crossing. In the case of the Y-component, this is most likely due to the aberration of the tail field relative to the GSM-coordinate system (if the tail is ~ 4° aberrated and the average Y-component in this coordinate system is assumed zero, a negative B_Y above and positive B_Y below the current sheet is expected in GSM-coordinates). However, the reason for the variation in B_Z is not so clear. In cases where the motion of the current sheet across the satellite is caused by external pressure pulses, the decrease in B_Z observed in 24 cases could be due to those effects. If the current sheet motion is due to internal dynamics, it is more difficult to explain the correlation between the sign reversals of the X and Z-components.

The average value of B_Z was calculated for each of the crossings by averaging B_Z-values 30 min before and after each crossing. The mean value was 0.24nT, with 9 events for which the 1-hour average

was negative, the smallest being -2.2nT. 15-min averages before and after the current sheet crossings gave mean values 0.56nT before and -0.18nT after the crossing, again showing the tendency for more negative B_Z after the crossing regardless of whether the satellite crossed the current sheet from the north or from the south. The anisotropic events had larger variation in the B_Z-components, larger positive B_Z before and more negative B_Z after the crossing. Magnetic activity strongly enhanced the probability of observing negative B_Z: For quiet events (hourly AE < 200nT) the average after the crossing was 0.31nT, whereas during more active events the average was -0.52nT. The current sheet thickness was not strongly correlated with the B_Z-values.

Discussion

The current carriers in these extremely thin current sheets, whether in the near-tail or in the distant tail, have not been conclusively identified. It is, however, important to understand how changes in the current sheet thickness and current carrying population affect the dynamical evolution of the tail during magnetically active periods. Mitchell et al. [1990] suggested that the cross-tail current in the thin current sheet during the substorm growth phase may be largely carried by the anisotropic electron population. Pulkkinen et al. [1992a] studied another event, where the electron current contribution, although present, was relatively small (~ 10% of the total current).

We have used the modified Harris equilibrium model B = $B_0 \tanh[U \cdot (t - t_0)/\lambda]x + B_n z$, where B_n is the magnetic field component normal to the current sheet, together with the field and electron data to estimate the electron current in the time-stationary limit. The average values of the lobe magnetic field and the electron plasma parameters were determined from the analyzed 33 crossings. Two values, an upper and a lower limit to the average magnetic field normal component (B_n) were defined. The upper limit to B_n was obtained by averaging over the absolute values of the measured B_Z-components and describes particle motion away from the X-point; the average of the actual B_Z values representing typical field values near the crossings was used as the lower limit. Correspondingly, this gives a lower and upper estimate for the current induced by the anisotropy in the electron distribution. When the modified Harris equilibrium field is used to calculate the gradient and curvature currents [Parker, 1957], the gradient current can be written in the form $j_G = [n_e(T_\parallel + T_\perp)/B_0\lambda]/\cosh^2(Z/\lambda)$, where n_e, $T_\parallel$, and $T_\perp$ are the electron density, parallel temperature, and perpendicular temperature, respectively. The curvature current is $j_C = [n_e(T_\parallel - T_\perp)/B_0\lambda]/\cosh^2(Z/\lambda)\cdot(B_0/B_N)^2/(1+(B_0/B_n)^2\tanh^2(Z/\lambda))$. Both currents are in the Y-direction. Figure 5 shows the total current density j = $\nabla \times$ B/μ_0, the electron gradient term, and the lower limit of the curvature term. The corresponding integrals over the current sheet thickness have been used to estimate how much of the current is carried by the electron population. On average, the gradient term gives 17 % of the current, whereas the contribution of the curvature term varies between 8 and 45 %, depending on how the average of the magnetic field normal component was chosen. As the normal component fluctuates around zero, the contribution of the curvature term may be strongly time dependent. It thus seems that the current carried by the electrons in many cases is large enough to be important to the tail dynamics.

Whether the tearing instability can grow in the thin current sheets is another question important both for the seemingly time-stationary distant tail configuration and the rapid evolution of the near-Earth tail during substorms. Pitch-angle scattering of thermal electrons has been suggested to trigger ion tearing in the near-Earth tail at substorm onset [Büchner and Zelenyi, 1987], leading to the disruption of the cross-tail current and formation of the substorm current wedge. The normal field component in the region close to 10R$_E$ during quiet times is sufficiently small to demagnetize the ions [West et al., 1978], but is large enough to keep the electrons magnetized. Recent magnetic field modeling results suggest that during the substorm growth phase the normal component is reduced sufficiently that the ~ 1 keV thermal electron population is scattered [Pulkkinen et al., 1992b].

In the distant tail the field configuration was frequently found to be close to or within the unstable regime and yet no current disruption events were found. In the Harris field model the condition for strong
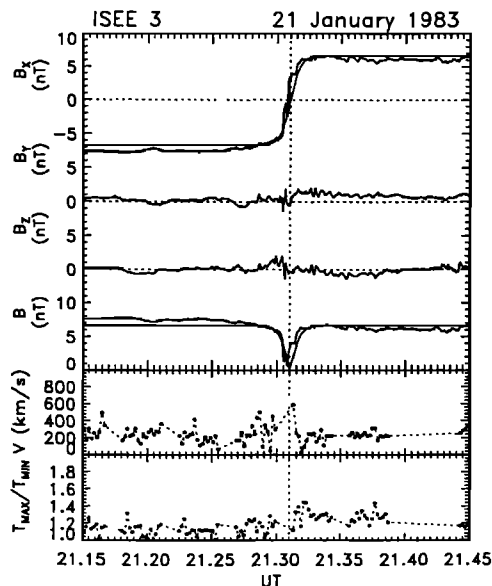

Fig. 4. Superposed epoch analysis for 33 current sheet crossings. The signs of both B_X and B_Y are reversed for south-to-north crossings, B_Z is unchanged for all crossings.
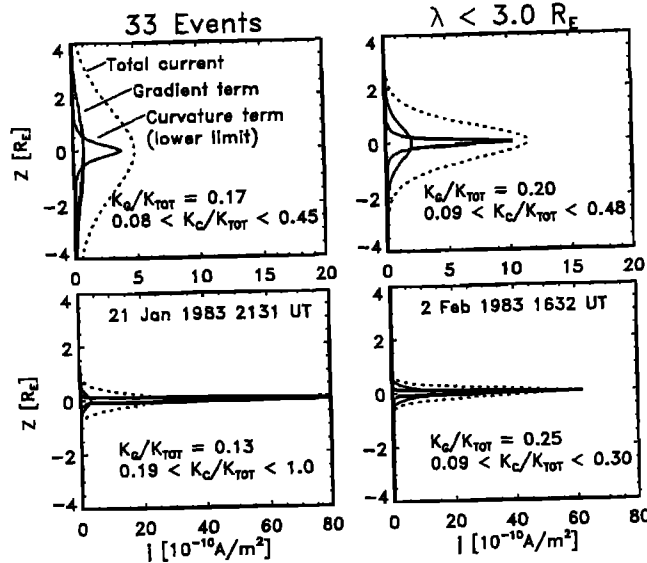
Fig. 5. Total current, electron gradient current, and curvature current for all 33 crossings (top left panel), for the thin current sheets ($\lambda < 3.0R_E$) (top right), and for two selected events, 21 January 1983, categorized as 'anisotropic' (lower left), and 2 February 1983, categorized as 'isotropic'. K_G, K_C, and K_{TOT} are the Z-integrated values of the electron gradient and curvature currents and the total current.

scattering can be written as $\kappa = (B_n/B_0)\sqrt{\lambda/\rho_{e,0}} \simeq 1$, where κ is the square root of the ratio between field line curvature radius and electron gyroradius, and $\rho_{e,0}$ is the electron gyroradius in the lobe field B_0. The average conditions in the distant tail described above give $\kappa = 1.1 - 8.6$ for 100eV electrons ($B_n = 0.15 - 1.14$nT). The corresponding value for the 100eV ions is $\kappa = 0.17 - 1.3$. Thus both the electrons and ions are close to the chaotic limit, with ions being on Speiser-type orbits when the normal component is sufficiently small, and the electrons being in the adiabatic regime when the normal component is large. This suggests that other effects, such as magnetic field radial gradients or the presence of heavier ions [Baker et al., 1982] may contribute to the instability onset in the near-Earth region.

We have studied 33 events where the ISEE 3 spacecraft crossed the current sheet in the deep geomagnetic tail. The current sheet was frequently found to be quite thin, in many cases only a fraction of an R_E. During the examined period (January 1983) there were in total 90 events where the spacecraft crossed the distant tail current sheet from one lobe to the other. Out of these 90 crossings 37 took place within 15 minutes and were thus selected to the original event list, and for 23 crossings we succeeded to determine the boundary velocity necessary for the current sheet thickness estimate. In 20 events the current sheet thickness was less than $3R_E$, and were characterized as thin current sheets. Thus, about 41% of the crossings took place within 15 minutes, and in 22% of all crossings were through a thin current sheet.

A superposed epoch analysis showed that the electron gradient term contributes relatively little to the cross-tail current, whereas the contribution of the curvature term may be quite substantial. The GEOTAIL mission recently launched to probe the same region of the tail with both ion and electron measurements available can bring valuable information on the current carriers and stability of thin one-dimensional current sheet structures.

References

Baker, D. N. and R. L. McPherron, Extreme energetic particle decreases near geostationary orbit: A manifestation of current diversion within the inner plasma sheet, J. Geophys. Res., 95, 6591, 1990.

Baker, D. N., et al., The possible role of ionospheric oxygen in the initiation and development of plasma sheet instabilities. Geophys. Res. Lett., 9, 1337, 1982.

Baker, D. N., et al., Average plasma and magnetic field variations in the distant magnetotail associated with near-Earth substorm effects, J. Geophys. Res., 92, 71, 1987.

Balogh, A., et al., The low-energy proton experiment on ISEE-C, IEEE Trans. Geosci. Electron., GE-16, 176, 1978.

Bame, S. J., et al., ISEE-C solar wind plasma experiment, IEEE Trans. Geosci. Electron., GE-16, 160, 1978.

Büchner, J. and L. M. Zelenyi, Chaotization of the electron motion as the cause of an internal magnetotail instability and substorm onset, J. Geophys. Res., 92, 13456, 1987.

Fairfield, D. H., et al., Multiple crossings of a very thin plasma sheet in the Earth's magnetotail, J. Geophys. Res., 86, 11189, 1981.

Frandsen, A. M. A., B. V. Connor, J. V. Amersfoort, and E. J. Smith, The ISEE-C vector helium magnetometer, IEEE Trans. Geosci. Electron., GE-16, 195, 1978.

Gosling, J. T., et al., North-south and dawn-dusk plasma asymmetries in the distant tail lobes: ISEE 3, J. Geophys. Res., 90, 6354, 1985.

McPherron, et al., Is near-Earth current sheet thinning the cause of auroral substorm onset?, in Y. Kamide and R. A. Wolf (eds): Quantitative modeling of magnetosphere-ionosphere coupling processes, Kyoto, Japan, 1987.

Mitchell, D. G., et al., Current carriers in the near-Earth cross-tail current sheet during substorm growth phase, Geophys. Res. Lett., 17, 583, 1990.

Murphy, N., et al., Enhancements of energetic ions associated with traveling compression regions in the deep geomagnetic tail, J. Geophys. Res., 92, 64, 1987.

Pulkkinen, T. I., et al., Global and local current sheet thickness estimated during the late growth phase, In: Substorms 1, ESA-SP 335, Noordwijk, The Netherlands, p. 131, 1992a.

Pulkkinen, T. I., et al., Particle scattering and current sheet stability in the geomagnetic tail during the substorm growth phase, J. Geophys. Res., 97, 19283, 1992b.

Slavin, J. A., et al., An ISEE-3 study of average and substorm conditions in the distant magnetotail, J. Geophys. Res., 90, 10,875, 1985.

West, H. I., Jr., et al., On the configuration of the magnetotail near midnight during quiet and weakly disturbed periods: State of the magnetosphere, J. Geophys. Res., 83, 3805, 1978.

Zwickl, R. D., et al., Evolution of the Earth's distant magnetotail: ISEE 3 electron plasma results, J. Geophys. Res., 89, 11,007, 1984.

T. I. Pulkkinen, Finnish Meteorological Institute, P.O.Box 503, SF-00101 Helsinki, Finland. Internet: Tuija.Pulkkinen@fmi.fi.

D. N. Baker and C. J. Owen, NASA/GSFC, Code 690, Greenbelt, MD 20771.

J. T. Gosling, Los Alamos National Laboratory, Los Alamos, NM 87545.

N. Murphy, Jet Propulsion Laboratory, Pasadena, CA 91109.